INSTITUTE OF PHYSICS PUBLISHING NONLINEARITY

Nonlinearity **14** (2001) 1239–1264 PII: S0951-7715(01)20866-4

Singularity formation in a class of stretched solutions of the equations for ideal magneto-hydrodynamics

J D Gibbon[1,2] **and K Ohkitani**[1]

[1] Research Institute for Mathematical Sciences, Kyoto University, Kyoto 606-8502, Japan
[2] Department of Mathematics, Imperial College of Science, Technology and Medicine, London SW7 2BZ, UK

Received 12 January 2001, in final form 19 June 2001
Published 6 August 2001
Online at stacks.iop.org/Non/14/1239

Recommended by S Fauve

Abstract

A class of stretched solutions of the equations for three-dimensional, incompressible, ideal magneto-hydrodynamics (MHD) is studied. In Elsasser variables, $\boldsymbol{V}^{\pm} = \boldsymbol{U} \pm \boldsymbol{B}$, these solutions have the form $\boldsymbol{V}^{\pm} = \left(\boldsymbol{v}^{\pm}, v_3^{\pm}\right)$ where $\boldsymbol{v}^{\pm} = \boldsymbol{v}^{\pm}(x, y, t)$ and $v_3^{\pm}(x, y, z, t) = z\gamma^{\pm}(x, y, t) + \beta^{\pm}(x, y, t)$. Two-dimensional partial differential equations for $\gamma^{\pm}$, $\boldsymbol{v}^{\pm}$ and $\beta^{\pm}$ are obtained that are valid in a tubular domain which is infinite in the z-direction with periodic cross section. Pseudo-spectral computations of these equations provide evidence for a blow-up in finite time in the above variables. This apparent blow-up is an infinite energy process that gives rise to certain subtleties; while all the variables appear to blow-up simultaneously, the two-dimensional part of the magnetic field $\boldsymbol{b} = \frac{1}{2}\left(\boldsymbol{v}^{+} - \boldsymbol{v}^{-}\right)$ blows up at a very late stage. This singularity in $\boldsymbol{b}$ is hard to detect numerically but supporting analytical evidence of a Lagrangian nature is provided for its existence. In three dimensions these solutions correspond to magnetic vortices developing along the axis of the tube prior to breakdown.

Mathematics Subject Classification: 35Q35, 76B03, 76W05

1. Introduction

The equations for three-dimensional (3D), incompressible ideal magneto-hydrodynamics (MHD) coupling of a magnetic field $\boldsymbol{B}(x, y, z, t)$ to an inviscid fluid are well known and take the form

$$\boldsymbol{U}_t + \boldsymbol{U} \cdot \nabla \boldsymbol{U} = \boldsymbol{B} \cdot \nabla \boldsymbol{B} - \nabla P \tag{1}$$

$$\boldsymbol{B}_t + \boldsymbol{U} \cdot \nabla \boldsymbol{B} = \boldsymbol{B} \cdot \nabla \boldsymbol{U} \tag{2}$$

$$\operatorname{div} \boldsymbol{U} = 0 \qquad \operatorname{div} \boldsymbol{B} = 0 \tag{3}$$

where $\boldsymbol{U}(x, y, z)$ is the fluid velocity and $P = p + \frac{1}{2}B^2$, where p is the hydrodynamic pressure. This coupling enhances the already formidable difficulties posed in understanding singularity formation in the three-dimensional incompressible Euler equations [1–3]. Beale *et al* identified $\int_0^t \|\boldsymbol{\omega}\|_\infty \, \mathrm{d}\tau$ as the quantity that controls singularities in the 3D Euler equations [1]. Using similar methods, Caflisch *et al* have shown that this must be extended to $\int_0^t (\|\boldsymbol{\omega}\|_\infty + \|\boldsymbol{J}\|_\infty) \, \mathrm{d}\tau$ for ideal MHD [4] where $\boldsymbol{J} = \operatorname{curl} \boldsymbol{B}$ is the current. Singularity formation is important because it has implications for reconnection processes in solar and astrophysics (see the two respective books by Biskamp [5] and by Priest and Forbes [6] and references therein). Kerr and Brandenburg [7] have numerically integrated equations (1)–(3), using 3D periodic boundary conditions, with two interlinked zero-velocity magnetic flux rings as initial data[1]. While they report that $\|\boldsymbol{J}\|_\infty$ grows very strongly, the evidence for it becoming singular is not conclusive. There are two papers that, respectively, report no blow-up in the two-dimensional [8] and three-dimensional cases [9]. Together these references suggest that the issue of singularity formation in the three-dimensional case is still open. There has been, however, some progress in the mathematical analysis of the two-dimensional problem (see, for example [10, 11]) but the possibility of two-dimensional blow-up has not been completely ruled out.

The purpose of this paper is to analyse solutions of (1)–(3) that may develop finite time singularities when the 3D domain has a tubular structure which is infinite in the z-direction, but periodic and finite in cross section $\mathcal{A} = [0, L]^2$. Clearly, such flows are neither finite in energy nor helicity so they fall into an entirely different category from the more familiar class of 3D finite domain flows whose energy and helicity are also finite [7, 9, 13]. Finally, we note that a different class of infinite energy solutions of the three-dimensional ideal MHD equations have been obtained in [12].

The idea is based on that developed by Gibbon *et al* [14] and Ohkitani and Gibbon [15], who examined a class of 3D Euler velocity fields of the form

$$\boldsymbol{U}(x, y, z, t) = \{u_1(x, y, t), \, u_2(x, y, t), \, z\gamma(x, y, t) + W(x, y, t)\} \tag{4}$$

where z appears only linearly in the third velocity component. It was shown in [14] that the variables $\gamma(x, y, t)$ and $W(x, y, t)$ and the third component of the vorticity $\omega(x, y, t) = u_{2,x} - u_{1,y}$ obey a simple set of coupled two-dimensional partial differential equations in which z plays no part. On a tubular domain which is infinite in z but periodic in cross section, Ohkitani and Gibbon [15] provided strong numerical evidence that the dominant variable γ develops a finite time singularity, thereby inducing the other variables to become singular. Two pieces of analytical work support this conclusion. Firstly, using rigorous analytical Lagrangian methods, Constantin [16] subsequently proved that this singularity in γ exists and that it must be two-sided; that is, from quite general initial data γ blows up simultaneously to $+\infty$ and $-\infty$ at different places in the cross sectional domain $\mathcal{A}$. The positive growth in γ is later and consequently steeper than the negative one. Secondly, Malham has shown that the support of negative regions of γ collapses to zero in a finite time, while the L^1-norm remains non-zero [17]. Ohkitani and Gibbon [15] also showed that the three-dimensional vortices that develop in the tube just before blow-up have a flower-like spatial structure, with petals of strong vorticity interleaved with hollow regions of weak vorticity. These vortices do not have finite energy and are destroyed when $\gamma \to \pm\infty$, indicating that the Euler equations will not sustain a solution of the form expressed in (4) past the singularity time.

Section 2 of this paper shows how a class of solutions of (1)–(3), similar to (4), can be found in Elsasser variables when the domain is also tubular. This doubles the number of variables in the problem over the Euler case; for instance, instead of the variables γ and

[1] In [7], the authors consider both the incompressible and compressible cases.

$\boldsymbol{u} = \{u_1, u_2\}$, there are now two in each case, $\gamma^{\pm}$ and $\boldsymbol{v}^{\pm}$. Nevertheless, as will be shown in section 3, the essential features displayed in the Euler calculations [15] are also present for ideal MHD. Both γ^+ and γ^- become singular in a finite time in a two-sided manner but, while they blow up simultaneously, their time evolution is generally not identical. The regions in which γ^+ and γ^- are negative in sign amplify strongly, while positive regions are flattened until, at a very late stage, blow-up occurs in their positive regions too. Additionally, the L^2-norms $\|\gamma^{\pm}\|_2$ also blow up simultaneously with $\|\gamma^{\pm}\|_\infty$. An unusual feature of the numerical calculations is the behaviour of the magnetic field. While there is evidence that it becomes singular simultaneously with the fluid variables, it remains small until a late stage and then grows in a very steep fashion. This late growth is hard to detect numerically, although it is supported by analytical evidence of a Lagrangian nature which is presented in section 2.3.

The type of singularity mechanism discussed in this paper, if it were to occur physically, would require infinite energy with particles being pulled from infinity. Such a process would violate the equations of motion, so our discussion of this mechanism should not be taken to be a literal claim that a true three-dimensional singularity would occur physically (see the discussion and references in [15]). More realistically, the types of solutions being discussed are those for which extremely strong growth occurs naturally and spontaneously from a large class of initial data. The jet-like 'magnetic vortices' that develop and open out along the axis of the tube before breakdown may have some application to astrophysics. These vortices dissolve once conditions for their existence have become invalid.

The doubling of the number of variables makes analysis much harder than in the 3D Euler case although certain results can be proved. In section 4 it is shown that both $\int_0^t \|\gamma^{\pm}\|_\infty \,\mathrm{d}\tau$ must either blow up simultaneously or remain bounded simultaneously. This is an analytical criterion against which numerical results can be tested: for instance, if one integral becomes singular and the other does not then the singularity must be an artefact of the numerical solution. These integrals, however, do not control potential singularities occurring in arbitrarily large gradients of γ or $\boldsymbol{v}^{\pm}$. It is shown in section 4 that the BKM criterion found by Caflisch *et al* [4] is replaced by one in terms of $\gamma^{\pm}$ and $\omega^{\pm} = |\operatorname{curl} \boldsymbol{v}^{\pm}|$; namely, that

$$\int_0^t \left(\|\gamma^+\|_\infty + \|\gamma^-\|_\infty + \|\omega^+\|_\infty + \|\omega^-\|_\infty\right) \mathrm{d}\tau \tag{5}$$

controls singularity formation in any variable.

2. The fundamental equations

2.1. Equations in Elsasser variables

It is well known that equations (1)–(3) for ideal MHD can be recast into a simpler form using Elsasser variables

$$\boldsymbol{V}^{\pm} = \boldsymbol{U} \pm \boldsymbol{B}. \tag{6}$$

With this combination, equations (1) and (2) become

$$\boldsymbol{V}_t^{\pm} + \boldsymbol{V}^{\mp} \cdot \nabla \boldsymbol{V}^{\pm} = -\nabla P \tag{7}$$

together with $\operatorname{div} \boldsymbol{V}^{\pm} = 0$. The linear z-structure of U_3 displayed in (4) can be used to good effect in (7). Take

$$\boldsymbol{V}^{\pm} = \left(\boldsymbol{v}^{\pm}, v_3^{\pm}\right) \tag{8}$$

where the two component vectors $\boldsymbol{v}^{\pm}$ are given by

$$\boldsymbol{v}^{\pm}(x, y, t) = \left\{v_1^{\pm}(x, y, t),\ v_2^{\pm}(x, y, t)\right\} \tag{9}$$

and

$$v_3^{\pm}(x, y, z, t) = z\gamma^{\pm}(x, y, t) + \beta^{\pm}(x, y, t). \tag{10}$$

With the $\pm$ two-dimensional material derivatives defined by

$$\frac{D^{\pm}}{Dt} = \frac{\partial}{\partial t} + \boldsymbol{v}^{\pm} \cdot \nabla \tag{11}$$

the velocity fields $\boldsymbol{v}^{\pm}$ satisfy[2]

$$\frac{D^{\mp}\boldsymbol{v}^{\pm}}{Dt} = -\nabla P \tag{12}$$

where ∇ is the two-dimensional gradient. The third component of (7) is more complicated but is the most important. Using the fact that

$$\left(\frac{\partial}{\partial t} + \boldsymbol{V}^{\mp} \cdot \nabla\right) z = v_3^{\mp} \tag{13}$$

the z-derivative of the pressure variable P is

$$\begin{aligned} -P_z &= \left(\frac{\partial}{\partial t} + \boldsymbol{V}^{\mp} \cdot \nabla\right) v_3^{\pm} \\ &= z\left(\frac{D^{\mp}\gamma^{\pm}}{Dt} + \gamma^{\pm}\gamma^{\mp}\right) + \left(\frac{D^{\mp}\beta^{\pm}}{Dt} + \gamma^{\pm}\beta^{\mp}\right). \end{aligned} \tag{14}$$

On integration with respect to z, P becomes

$$-P(x, y, z, t) = \frac{1}{2}z^2\left(\frac{D^{\mp}\gamma^{\pm}}{Dt} + \gamma^{\pm}\gamma^{\mp}\right) + z\left(\frac{D^{\mp}\beta^{\pm}}{Dt} + \gamma^{\pm}\beta^{\mp}\right) + f(x, y, t). \tag{15}$$

Because the partial derivatives P_x and P_y in (12) do not contain z, the only way to avoid a contradiction between (12) and (15) is to have the two main terms in round brackets on the right-hand side of (15) uniform in space so they vanish under derivatives in x and y. Hence

$$\frac{D^{\mp}\gamma^{\pm}}{Dt} + \gamma^{\pm}\gamma^{\mp} = -P_{zz}(t) \tag{16}$$

where $P_{zz}(t)$ is an arbitrary function of time but is uniform in space. Also

$$\frac{D^{\mp}\beta^{\pm}}{Dt} + \gamma^{\pm}\beta^{\mp} = 0. \tag{17}$$

An arbitrary function of time could have been placed on the right-hand side of (17) but this has been put to zero because it is no more than an arbitrary acceleration in the z-direction. This is the generalization to ideal MHD of the ideas in [14].

[2] Note that the sign label on the material derivative is opposite to the function on which it is operating.

2.2. Two-dimensional equations for $\gamma^{\pm}$, $\boldsymbol{v}^{\pm}$ and $\beta^{\pm}$ on a tubular domain

The equations for $\gamma^{\pm}$, $\boldsymbol{v}^{\pm}$ and $\beta^{\pm}$ have not, as yet, had any boundary conditions applied, thereby leaving $P_{zz}(t)$ arbitrary. Let us designate the full three-dimensional domain as a tube, infinite in the z-direction, with a finite cross section as $\mathcal{A} = [0,\ L]^2$ with periodic boundary conditions applying across it. The key point is that the two three-dimensional divergence-free conditions $\operatorname{div} \boldsymbol{V}^{\pm} = 0$ in two dimensions become

$$\operatorname{div} \boldsymbol{v}^{\pm} = -\gamma^{\pm}. \tag{18}$$

Integration of (18) across $\mathcal{A}$ implies that $\gamma^{\pm}$ must satisfy the pair of mean-zero conditions

$$\int_{\mathcal{A}} \gamma^{\pm} \,\mathrm{d}\boldsymbol{x} = 0. \tag{19}$$

Applying these mean-zero conditions to (16) determines $P_{zz}(t)$

$$\frac{D^{\mp}\gamma^{\pm}}{Dt} + \gamma^{\pm}\gamma^{\mp} = 2L^{-2} \int_{\mathcal{A}} \gamma^{\pm}\gamma^{\mp} \,\mathrm{d}\boldsymbol{x}. \tag{20}$$

This pair, together with the equations for $\boldsymbol{v}^{\pm}$ and $\beta^{\pm}$

$$\frac{D^{\mp}\boldsymbol{v}^{\pm}}{Dt} = -\nabla P \tag{21}$$

$$\frac{D^{\mp}\beta^{\pm}}{Dt} = -\gamma^{\pm}\beta^{\mp} \tag{22}$$

constitute a double set of equations that are almost the generalization of those found for 3D Euler in [15]. What is missing from equations (18)–(22), and what differs from the Euler case, is that there is no pair of independent equations for $\omega^{\pm} = \boldsymbol{k} \cdot \operatorname{curl} \boldsymbol{v}^{\pm}$ ($\boldsymbol{k}$ is a unit vector in the z-direction) because of the extra complication that occurs when the curl is taken of $\boldsymbol{v}^{\mp} \cdot \nabla \boldsymbol{v}^{\pm}$. In the Euler case in [15] it was possible to reconstruct $\boldsymbol{u}$ from the equations for γ and ω via a Hodge decomposition without having to integrate the velocity equations directly. A direct numerical integration of (21) to find $\boldsymbol{v}^{\pm}$ is unavoidable here. In turn, this means solving for the Laplacian of the pressure, which can be found by taking the 2D divergence of (21),

$$-\Delta P = \sum_{i,j} v^{\pm}_{i,j} v^{\mp}_{j,i} + \gamma^{\pm}\gamma^{\mp} - 2L^{-2} \int_{\mathcal{A}} \gamma^{\pm}\gamma^{\mp} \,\mathrm{d}\boldsymbol{x} \tag{23}$$

where Δ is the 2D Laplacian. Equation (20) has been used to derive (23), which is invariant under the exchange $\pm \to \mp$. A simple pair of relationships for $\omega^{\pm}$ can be found through their definitions

$$\omega^{\pm} = v^{\pm}_{2,x} - v^{\pm}_{1,y} \tag{24}$$

for which it is easily shown that

$$\frac{D^{-}\omega^{+}}{Dt} = \gamma^{-}\omega^{+} + J_{x,y}(v^{+}_{1},\ v^{-}_{1}) + J_{x,y}(v^{+}_{2},\ v^{-}_{2}). \tag{25}$$

The Jacobian terms can be eliminated by the addition of (25) with its equivalent for ω^{-} to give

$$\frac{D^{-}\omega^{+}}{Dt} + \frac{D^{+}\omega^{-}}{Dt} = \gamma^{-}\omega^{+} + \gamma^{+}\omega^{-}. \tag{26}$$

It is obvious from (25) and (26) that $\int_{\mathcal{A}} \omega^{\pm} \,\mathrm{d}\boldsymbol{x} =$ constant, which simply means that the fluid and magnetic circulations are constant.

The case closest to 3D Euler, but not identical to it, is that of force-free state in the sense that the Lorentz force reduces to a gradient. Here the magnetic field is taken to be $\boldsymbol{B} = (0,\ 0,\ B_3)$. Taking $\gamma^+ = \gamma^- = \gamma$, $\boldsymbol{v}^+ = \boldsymbol{v}^- = \boldsymbol{v}$ and $\beta^\pm = W \pm B_3$, equation (22) reduces to two equations

$$\frac{DW}{Dt} = -\gamma W \qquad \frac{DB_3}{Dt} = \gamma B_3. \tag{27}$$

The equation for B_3 is just one extra on top of those for 3D Euler.

2.3. A material treatment of the magnetic field

Consider the two-dimensional basic variables

$$\boldsymbol{u} = \frac{\boldsymbol{v}^+ + \boldsymbol{v}^-}{2} \qquad \boldsymbol{b} = \frac{\boldsymbol{v}^+ - \boldsymbol{v}^-}{2} \tag{28}$$

in the decomposition $\boldsymbol{v}^\pm = \boldsymbol{u} \pm \boldsymbol{b}$. The equation for the two-dimensional part of the magnetic field $\boldsymbol{b}$ reads

$$\frac{D\boldsymbol{b}}{Dt} = \boldsymbol{b} \cdot \nabla \boldsymbol{u} \tag{29}$$

which has an integral (Cauchy formula) of the form

$$\boldsymbol{b} = \boldsymbol{b}_0 \cdot \frac{\partial}{\partial \boldsymbol{a}} \boldsymbol{x} \tag{30}$$

where $\boldsymbol{b}_0$ is the initial magnetic field and $\boldsymbol{a}$ is a Lagrangian particle label $\boldsymbol{a} = (\xi,\ \eta)$. The determinant of the Jacobian matrix

$$J = \frac{\partial(x,\ y)}{\partial(\xi,\ \eta)} \tag{31}$$

satisfies

$$\frac{DJ}{Dt} = -\gamma J \tag{32}$$

where $\gamma = (\gamma^+ + \gamma^-)/2$ and the total derivative is simply $\partial_t + \boldsymbol{u} \cdot \nabla$. It follows that

$$J(\boldsymbol{a}, t) = \exp\left(-\int_0^t \gamma(\boldsymbol{a}, s)\, \mathrm{d}s \right) \tag{33}$$

for $J(\boldsymbol{a}, 0) = 1$. Hence, if $\gamma \to -\infty$ in a finite time, then $J \to \infty$ at the same time. Therefore, some components of the Jacobian matrix $\partial x_i/\partial\xi,\ \partial x_i/\partial\eta$ $(i = 1, 2)$ must also be singular at that time. From (30) this establishes the important result that $\boldsymbol{b}$ must also become singular if there is negative blow-up in γ, except for a very slim possibility that the product with $\boldsymbol{b}_0$ accidentally cancels the singular contributions. This simultaneous blow-up in γ and $\boldsymbol{b}$ will be discussed further in the next section when the numerical calculations are considered.

3. Numerical results

A standard pseudo-spectral method was employed to solve equations (12) and (23). The aliasing error was eliminated by the $\frac{2}{3}$-rule and so the maximum wavenumber took the value $N/3$ for a computation with N^2 grid points. Values taken for N were 256, 512 and 1024. Time marching was performed using a fourth-order Runge–Kutta scheme with a typical time increment $\Delta t = 10^{-3}$. Two types of initial conditions were used; simple sinusoidal data and random initial data. Numerical results can mainly be described using $N = 256$ because no qualitative difference appeared at higher resolutions.

3.1. A simple sinusoidal initial condition (IC 1)

Consider a simple initial condition for $\gamma^{\pm}$ of the form

$$\gamma^{+} = \sin x \sin 2y \qquad \gamma^{-} = \sin 2x \sin y. \tag{34}$$

The velocity fields corresponding to these

$$v_1^{+} = \tfrac{3}{10}\sin(x+2y) + \tfrac{1}{10}\sin(x-2y) \qquad v_2^{+} = \tfrac{1}{10}\sin(x+2y) + \tfrac{3}{10}\sin(x-2y) \tag{35}$$

$$v_1^{-} = \tfrac{3}{10}\sin(2x+y) - \tfrac{1}{10}\sin(2x-y) \qquad v_2^{-} = -\tfrac{1}{10}\sin(2x+y) + \tfrac{3}{10}\sin(2x-y) \tag{36}$$

are obtained by solving

$$v_1^{\pm} = -\triangle^{-1}\left(\frac{\partial \gamma^{\pm}}{\partial x} + \frac{\partial \omega^{\pm}}{\partial y}\right) \tag{37}$$

$$v_2^{\pm} = \triangle^{-1}\left(\frac{\partial \omega^{\pm}}{\partial x} - \frac{\partial \gamma^{\pm}}{\partial y}\right). \tag{38}$$

Spatial averages of squared field variables are defined as follows:

$$E^{\pm}(t) = \frac{1}{2L^2}\int_{\mathcal{A}} |\boldsymbol{v}^{\pm}|^2 \,\mathrm{d}\boldsymbol{x} \tag{39}$$

$$E_{\omega}^{\pm}(t) = \frac{1}{2L^2}\int_{\mathcal{A}} |\omega^{\pm}|^2 \,\mathrm{d}\boldsymbol{x} \tag{40}$$

$$E_{\gamma}^{\pm}(t) = \frac{1}{2L^2}\int_{\mathcal{A}} |\gamma^{\pm}|^2 \,\mathrm{d}\boldsymbol{x} \tag{41}$$

$$E_{\beta}^{\pm}(t) = \frac{1}{2L^2}\int_{\mathcal{A}} |\beta^{\pm}|^2 \,\mathrm{d}\boldsymbol{x}. \tag{42}$$

The time evolution of these norms are shown in figure 1(*a*). For this particular initial condition, the norms of + fields are found to be identical to those of − fields; that is, $E^{+}(t) = E^{-}(t)$ for all t. Similar kinds of equalities hold for ω, γ and β as well. Hence, as far as the norms are concerned, the superscripts will be dropped in this subsection, although such relations do not hold in general. It is seen in figure 1(*a*) that these norms differ in their growth rates; $E(t)$ and $E_{\gamma}(t)$ clearly grow more rapidly than $E_{\omega}(t)$ and that $E_{\beta}(t)$ grows least rapidly of all. However, it should be noted that they apparently diverge at the same time $t_* = 1.6$.

To quantify the strength of the singularity, log–log plots are shown near $t = t_*$ in figure 1(*b*). It is clear from this figure that the apparent singularities in $E(t)$ and $E_{\gamma}(t)$ are stronger than those in $E_{\omega}(t)$ and $E_{\beta}(t)$. In fact, a power-law behaviour is not obvious, possibly because of the presence of logarithmic contributions. As the exact forms of such contributions are unknown we have refrained from fitting them by trial functions; rather, two straight lines have been inserted in the figure as guidelines. Using these rough estimates it is observed that in the range $0.005 \leqslant t_* - t \leqslant 0.1$

$$E(t) \propto \frac{1}{(t_*-t)^{\alpha}} \qquad E_{\omega}(t) \propto \frac{1}{(t_*-t)^{\alpha_{\omega}}} \tag{43}$$

$$E_{\gamma}(t) \propto \frac{1}{(t_*-t)^{\alpha_{\gamma}}} \qquad E_{\beta}(t) \propto \frac{1}{(t_*-t)^{\alpha_{\beta}}} \tag{44}$$

may be good approximations with exponents

$$\alpha \approx 2 \qquad \alpha_{\omega} \approx 1.5 \qquad \alpha_{\gamma} \approx 2 \qquad \alpha_{\beta} \approx 1.5. \tag{45}$$

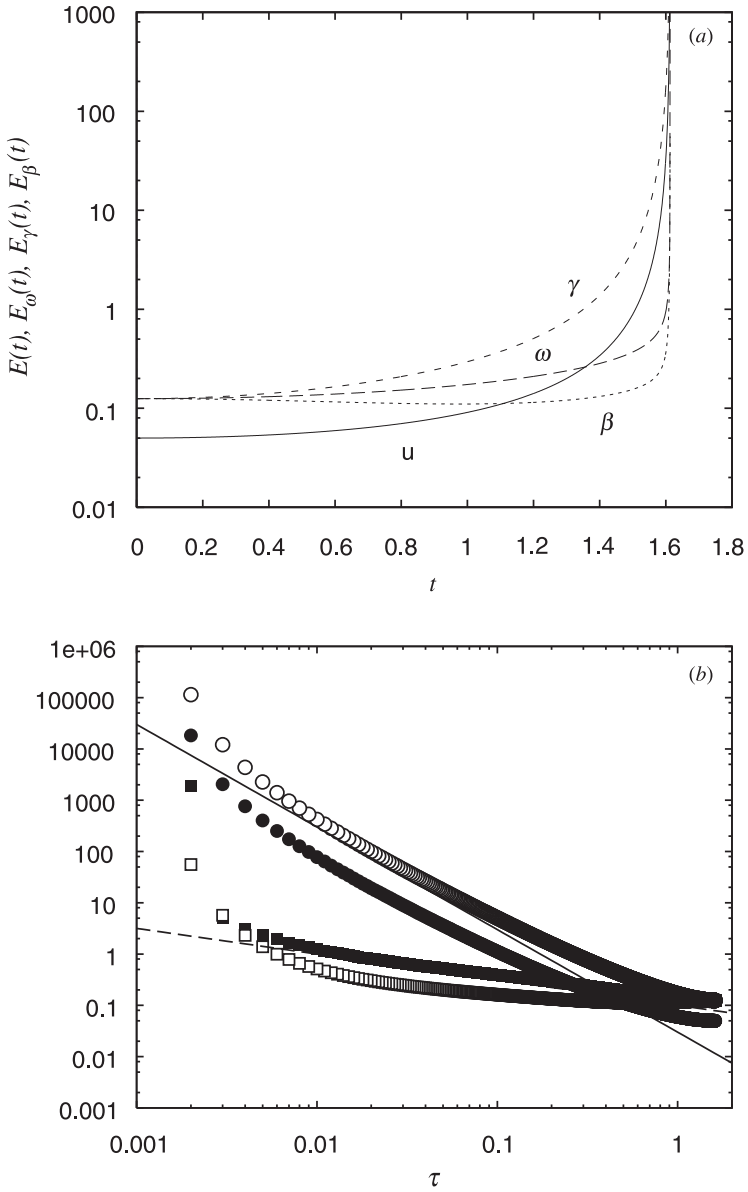

Figure 1. (*a*) The time evolution of $E(t)$ (full), $E_\omega(t)$ (long-broken), $E_\gamma(t)$ (short-broken) and $E_\beta(t)$ (dotted). (*b*) The time evolution of $E(t)$ (full circles), $E_\omega(t)$ (full squares), $E_\gamma(t)$ (open circles) and $E_\beta(t)$ (open squares). The full curve represents τ^{-2} and the broken one $\tau^{-1.5}$.

In order to understand the formation of an apparent singularity the spatial structure of the two-dimensional domain is examined next. The time evolution of the perspective plots of γ^+ and γ^- are shown, respectively, in figures 2(*a*) and (*b*). Note that both have the same L^2-norms and L^∞-norms; $E_\gamma^+(t) = E_\gamma^-(t)$ and $\max_{\boldsymbol{x}} \gamma^+(\boldsymbol{x}, t) = \max_{\boldsymbol{x}} \gamma^-(\boldsymbol{x}, t)$ and $\min_{\boldsymbol{x}} \gamma^+(\boldsymbol{x}, t) = \min_{\boldsymbol{x}} \gamma^-(\boldsymbol{x}, t)$. It should also be noted that in general $\gamma^+(x, y)$ is *not* obtained from $\gamma^-(x, y)$ by simply exchanging the argument variables x and y, even though this is true initially. As time evolves negative spikes become prominent in both fields and it is noticeable

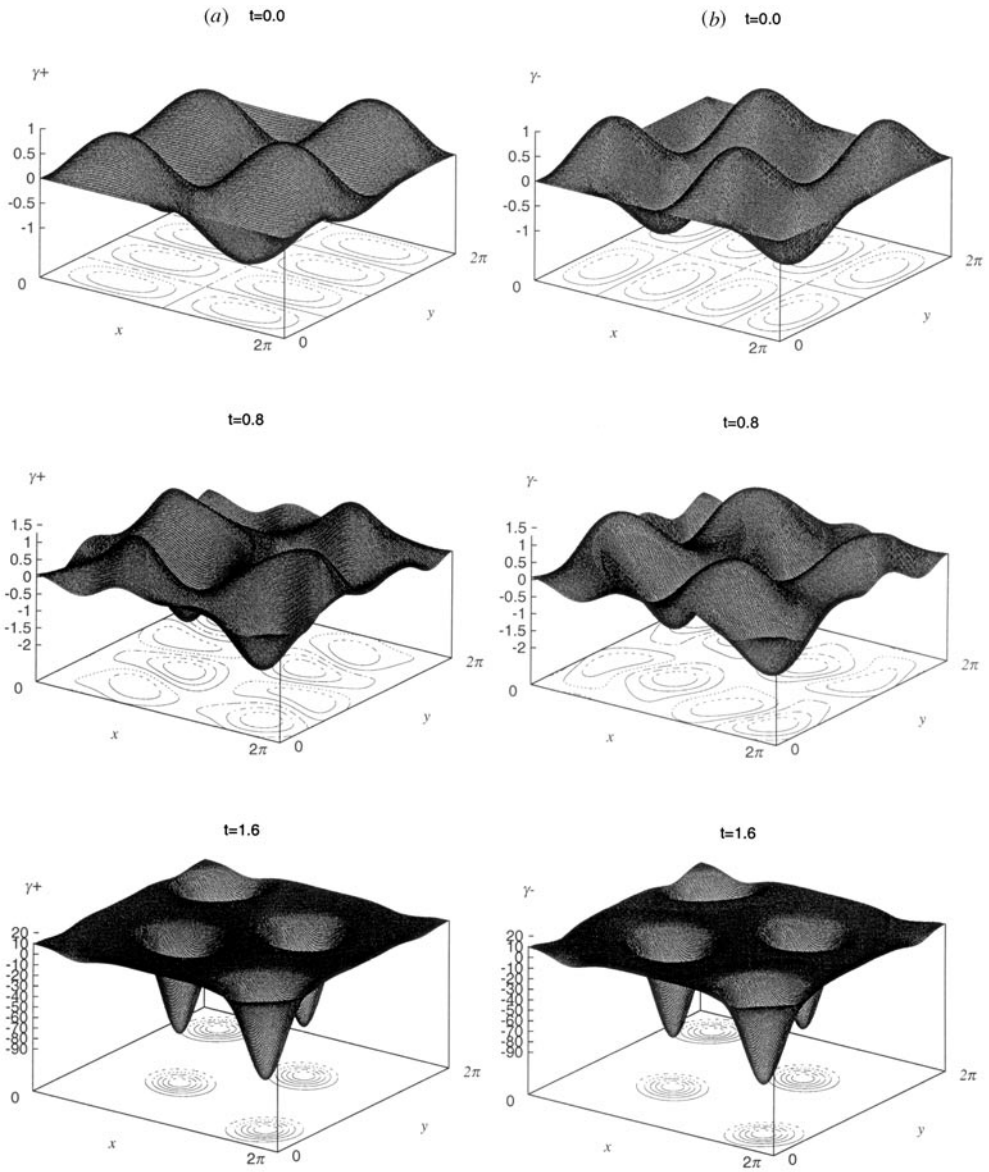

Figure 2. (*a*) Perspective plots of γ^+ at $t = 0, 0.8, 1.6$. Five levels of contours are drawn with an equal increment between the maximum and the minimum. (*b*) Similar perspective plots of γ^-.

that at $t = 1.6$ these peaks are located at almost the same positions. In fact, the normalized correlation coefficient between γ^+ and γ^-, defined by

$$C_\gamma(t) = \frac{\int_{\mathcal{A}} \gamma^+\gamma^- \,\mathrm{d}\boldsymbol{x}}{\left(\int_{\mathcal{A}} (\gamma^+)^2 \,\mathrm{d}\boldsymbol{x} \int_{\mathcal{A}} (\gamma^-)^2 \,\mathrm{d}\boldsymbol{x}\right)^{1/2}} \tag{46}$$

is close to unity at late times (see figure 3), with $C_\gamma(t) = 0.98$ at $t = 1.6$. In the later stages $C_\gamma(t)$ behaves linearly in t. It is also shown in the same figure time evolution of the normalized

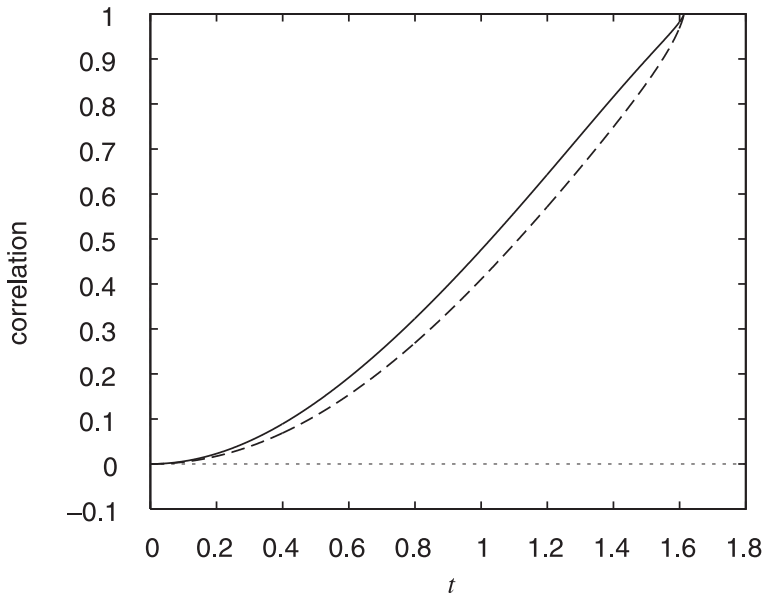

Figure 3. The normalized correlation coefficient between γ^+ and γ^- (full) and $\boldsymbol{v}^+$ and $\boldsymbol{v}^-$ (broken). The dotted line denotes zero.

correlation coefficient between $\boldsymbol{v}^+$ and $\boldsymbol{v}^-$

$$C_v(t) = \frac{\int_{\mathcal{A}} \boldsymbol{v}^+ \cdot \boldsymbol{v}^- \, \mathrm{d}\boldsymbol{x}}{\left(\int_{\mathcal{A}} (\boldsymbol{v}^+)^2 \, \mathrm{d}\boldsymbol{x} \int_{\mathcal{A}} (\boldsymbol{v}^-)^2 \, \mathrm{d}\boldsymbol{x}\right)^{1/2}}. \tag{47}$$

It is a little smaller than $C_\gamma(t)$ but is very close to unity in the later stages, that is, $C_v(t) = 0.97$ at $t = 1.6$. One is tempted to think naively that $\gamma^+ \to \gamma^-$ as the critical time t_* is approached. However, this is not the case, because a singularity forms concomitantly in the magnetic field that contradicts such a simple interpretation (see below).

In figures 4(a) and (b) perspective plots of ω^+ and ω^- are shown. Their increase in magnitude is less prominent than that of $\gamma^\pm$, but they clearly form platform-like structures around $t = 1.6$, although each respective structure is located in different regions.

In figure 5(a) the time evolution of the maximum value of $|\boldsymbol{v}^+|$ and the maximum and minimum values of γ^+ are plotted against $\tau = t_* - t$ on a log–log plot. In figure 5(a) the straight line has a slope of $(t_* - t)^{-1}$ and we see that $-\min_{\boldsymbol{x}} \gamma^+(\boldsymbol{x}, t)$ shows stronger singular behaviour. This is consistent with the BKM-type analysis presented in section 4. Note that the maximum and minimum values of γ^+ are equal to those of γ^-, respectively. We also show similar plots for $\omega^\pm$ and $\beta^\pm$ in figures 5(b) and (c). For the maximum and minimum of $\omega^\pm$ and $\beta^\pm$, the power-law behaviour is not clearly observed. Still, it is clearly seen that a singular behaviour in $\omega^\pm$ is much weaker than that of $\gamma^\pm$. A power-law behaviour is only observed in the very late stage of development in $\max_{\boldsymbol{x}} \omega^+$, $\max_{\boldsymbol{x}} \omega^-$. The same is true for $\max_{\boldsymbol{x}} \beta^+$, $-\min_{\boldsymbol{x}} \beta^+$. In the late stage, they agree in the interval $t_* - t < 0.01$, which means that in the late stage only one particular structure dominates, whereas in the earlier stage a number of structures at different locations contribute to the maximum values. We note also that the maximum and minimum values of β^+ are equal to those of β^-, respectively. Moreover, we have $\max_{\boldsymbol{x}} \omega^+(\boldsymbol{x}, t) = -\min_{\boldsymbol{x}} \omega^+(\boldsymbol{x}, t)$ for this particular initial condition.

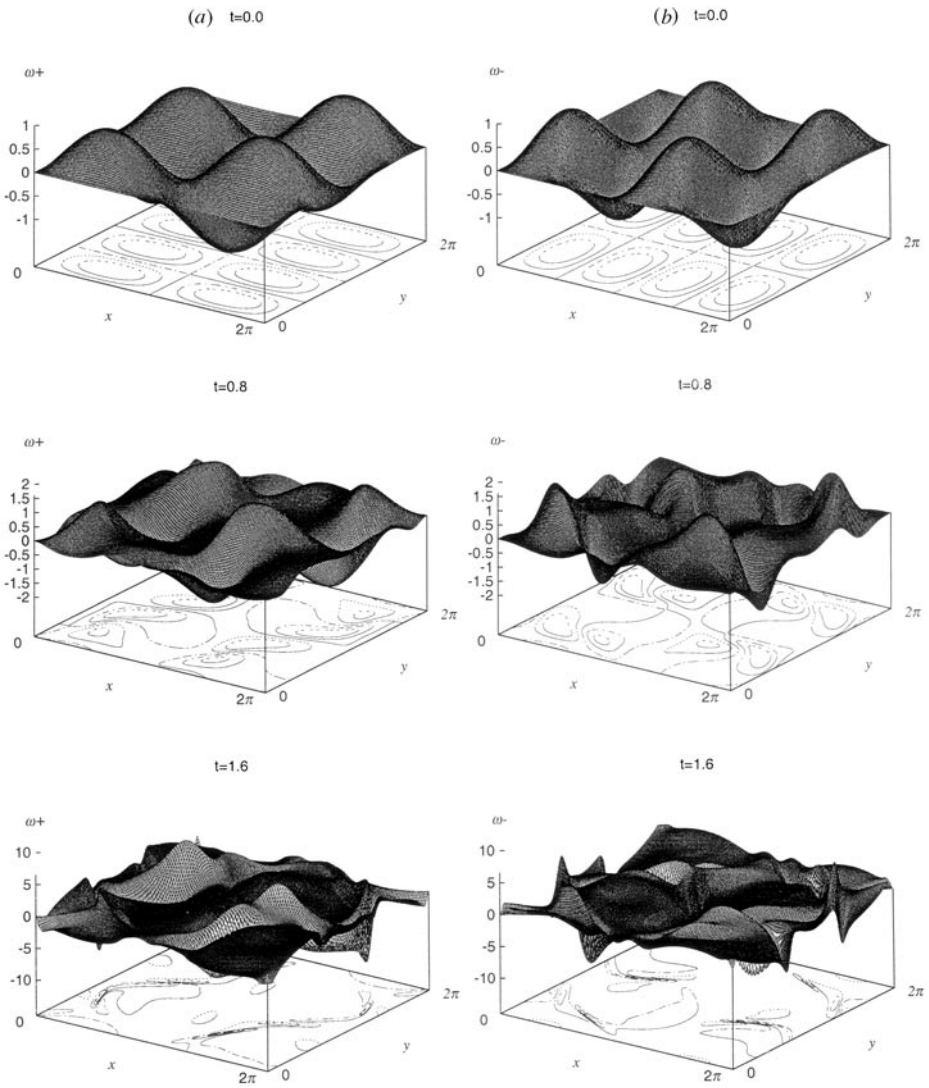

Figure 4. (*a*) Perspective plots of ω^+ at $t = 0, 0.8, 1.6$. (*b*) Similar perspective plots of ω^-.

Now we consider the magnetic field. The total kinetic and magnetic energy on the two-dimensional domain $\mathcal{A}$ are given by

$$E_u(t) = \frac{1}{2L^2}\int_{\mathcal{A}} |\boldsymbol{u}|^2 \,\mathrm{d}\boldsymbol{x} \qquad E_b(t) = \frac{1}{2L^2}\int_{\mathcal{A}} |\boldsymbol{b}|^2 \,\mathrm{d}\boldsymbol{x}. \tag{48}$$

Their time evolution is shown in figure 6(*a*). While initially both energies are identical, the kinetic energy $E_u(t)$ grows much more rapidly than $E_b(t)$. Both of these quantities blow up simultaneously but figure 6(*a*) shows that $E_b(t)$ remains small until a very late stage after which it grows in a very steep manner. In figure 6(*b*) the time evolution is shown of the maximum values of $|\boldsymbol{u}|$ and $|\boldsymbol{b}|$

$$\|\boldsymbol{u}\|_\infty = \max_{\boldsymbol{x}} |\boldsymbol{u}(\boldsymbol{x}, t)| \qquad \|\boldsymbol{b}\|_\infty = \max_{\boldsymbol{x}} |\boldsymbol{b}(\boldsymbol{x}, t)|. \tag{49}$$

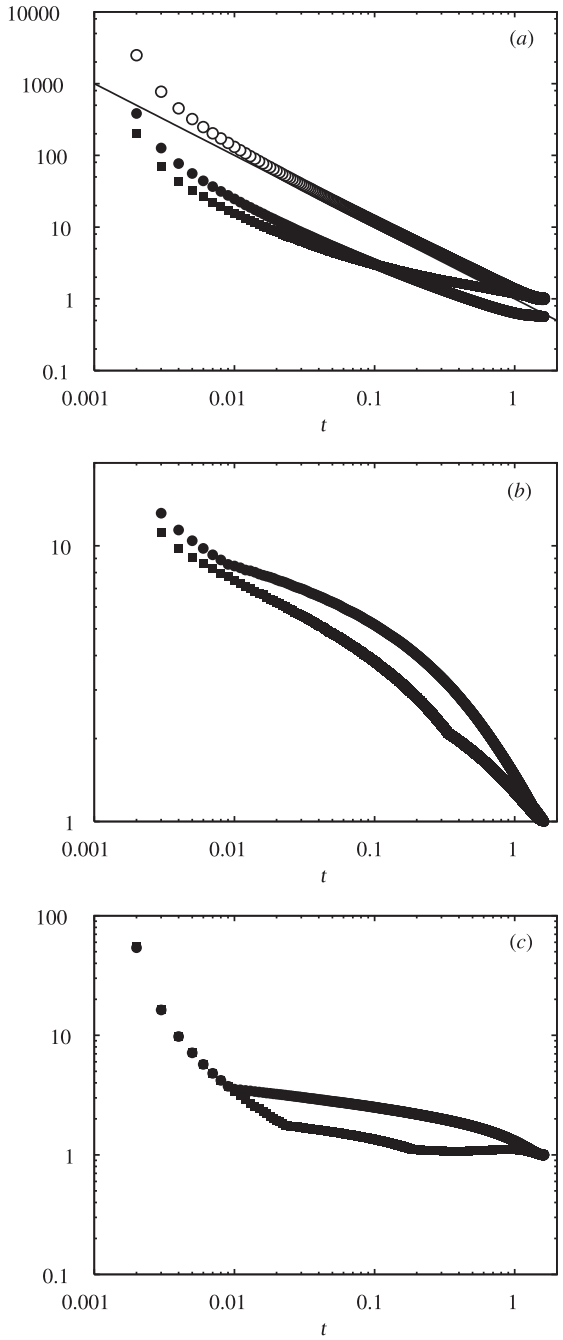

Figure 5. (*a*) Time evolution of the maximum and minimum values: $\max_x |\boldsymbol{v}^+|(\boldsymbol{x}, t)$ (full squares), $\max_x \gamma^+(\boldsymbol{x}, t)$ (full circles), and $-\min_x \gamma^+(\boldsymbol{x}, t)$ (open squares). The full line represents a slope τ^{-1}. Note that $\max_x \gamma^+(\boldsymbol{x}, t) = \max_x \gamma^-(\boldsymbol{x}, t)$ for this initial condition. (*b*) Time evolution of the maximum values: $\max_x \omega^+(\boldsymbol{x}, t)$ (circles) and $\max_x \omega^-(\boldsymbol{x}, t)$ (squares). Note that $\max_x \omega^+(\boldsymbol{x}, t) = -\min_x \omega^+(\boldsymbol{x}, t)$ for this initial condition. (*c*) Time evolution of the maximum and minimum values: $\max_x \beta^+(\boldsymbol{x}, t)$ (full circles) and $-\min_x \beta^+(\boldsymbol{x}, t)$ (full squares). Note that $\max_x \beta^+(\boldsymbol{x}, t) = \max_x \beta^-(\boldsymbol{x}, t)$ for this initial condition.

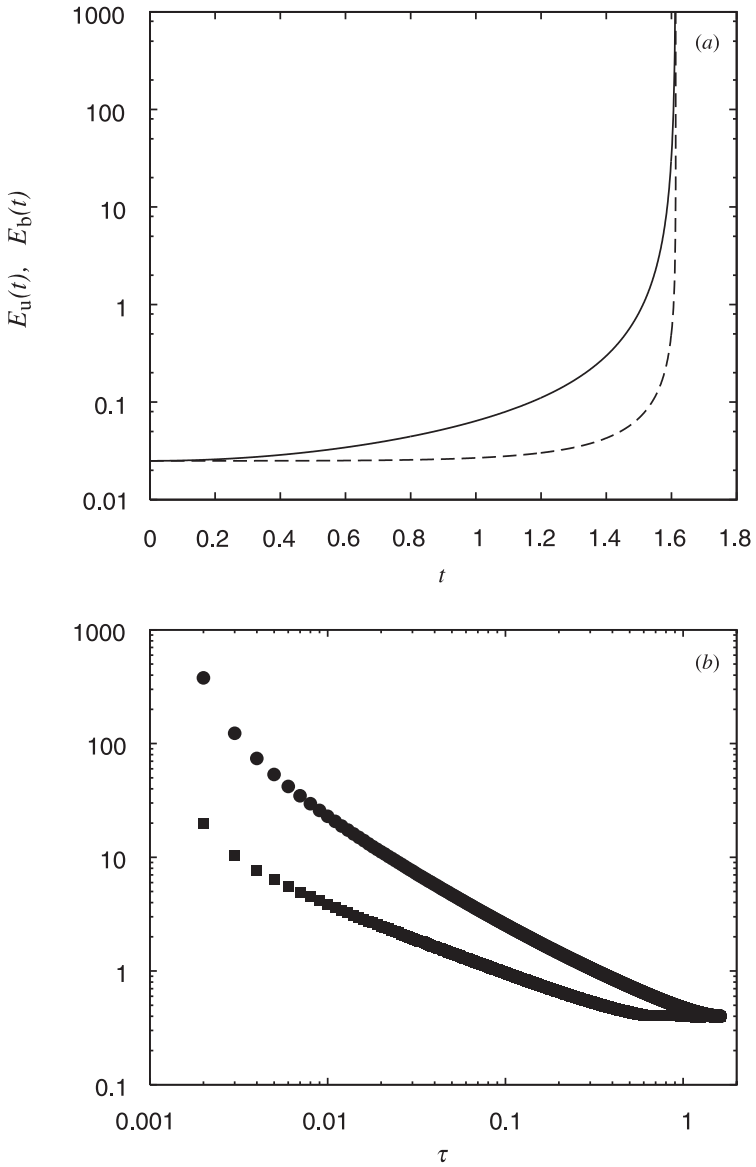

Figure 6. (*a*) Time evolution of the total kinetic energy $E_u(t)$ (full) and magnetic energy $E_b(t)$ (broken). (*b*) Time evolution of the maximum values of $\max_x |\boldsymbol{u}|$ (full circles) and $\max_x |\boldsymbol{b}|$ (full squares).

Just as in the L^2-norms, $\|\boldsymbol{b}\|_\infty$ does not increase significantly in the early stage but both norms grow rapidly in the end.

This apparent late growth in $\|\boldsymbol{b}\|_\infty$ requires some discussion because it is associated with an important mechanism regarding the magnetic field. A naive interpretation of the behaviour of the correlation functions (46) and (47), as well as the plots in figures 2(*a*), (*b*) and 3, would

be to believe that $\gamma^+ \to \gamma^-$ and $\boldsymbol{v}^+ \to \boldsymbol{v}^-$ *pointwise*. If this were the case then the relations

$$\int_{\mathcal{A}} |\boldsymbol{b}|^2 \, \mathrm{d}\boldsymbol{x} = 4 \int_{\mathcal{A}} (\boldsymbol{v}^+ - \boldsymbol{v}^-)^2 \, \mathrm{d}\boldsymbol{x} \tag{50}$$

and

$$\int_{\mathcal{A}} (\operatorname{div} \boldsymbol{b})^2 \, \mathrm{d}\boldsymbol{x} = 4 \int_{\mathcal{A}} \left(\gamma^+ - \gamma^-\right)^2 \, \mathrm{d}\boldsymbol{x} \tag{51}$$

would imply that $\boldsymbol{b} \to 0$ and $\operatorname{div} \boldsymbol{b} \to 0$ at every point in $\mathcal{A}$, showing that the fluid would dominate over the magnetic field, which would die out as $t \to t_*$. The situation is more subtle than this because such a result would contradict a blow-up in $\boldsymbol{b}$. In fact, it was shown in equation (33) in section 2.3, that $\boldsymbol{b}$ must become singular as $\gamma^\pm \to -\infty$. The very late growth observed in E_b in figure 6(a) is consistent with this. Also consistent with this observation are the distinct differences in the plots of ω^+ and ω^- (see figures 4(a), and (b)) indicating that $\boldsymbol{v}^+$ and $\boldsymbol{v}^-$ are not identical near t_*. Unfortunately, the growth in $\|\boldsymbol{b}\|_\infty$ is so late that only an amplification factor of the order of 10 was achieved over initial data (see figure 6(b)). It is possible that $\|\boldsymbol{b}\|_\infty$ blows up at a different (i.e. slower) rate than that for $\|\boldsymbol{u}\|_\infty$ (we are grateful to Professor Okamoto for suggesting this possibility). However, it seems impossible to conclude that this is the case from the present calculations. More detailed numerical work at much higher resolutions closer to t_* might shed some light on the details of this apparent growth in $\|\boldsymbol{b}\|_\infty$.

We show the evolution of perspective plots of $|\boldsymbol{b}|^2$ and j in figures 7(a) and (b), respectively, which are defined by

$$\boldsymbol{b} = \frac{\boldsymbol{v}^+ - \boldsymbol{v}^-}{2} \qquad j = \frac{\partial b_2}{\partial x_1} - \frac{\partial b_1}{\partial x_2}. \tag{52}$$

At $t = 1.6$ intense $|\boldsymbol{b}|$ regions take an almost circular form, with current sheets developing around them. This is reminiscent of the characteristic structure in the two-dimensional MHD problem (see, for example, Sulem *et al* [18]).

Since the solution under consideration is three dimensional in nature, it is of interest to observe the full three-dimensional structure in a box $[0, L]^3$. The 3D iso-surfaces of $|\boldsymbol{U}|^2$ and $|\boldsymbol{\Omega}|^2$ are shown in figures 8(a) and (b), respectively. We recall that

$$\boldsymbol{U} = \tfrac{1}{2}\left(\boldsymbol{V}^+ + \boldsymbol{V}^-\right) = \tfrac{1}{2}\left(\boldsymbol{v}^+ + \boldsymbol{v}^-, \, z\left(\gamma^+ + \gamma^-\right) + \beta^+ + \beta^-\right) \tag{53}$$

and

$$\boldsymbol{\Omega} = \nabla \times \boldsymbol{U}. \tag{54}$$

Also shown are the iso-surfaces of $|\boldsymbol{B}|^2$ and $|\boldsymbol{J}|^2$ in figures 8(c) and (d), respectively. Note that

$$\boldsymbol{B} = \tfrac{1}{2}\left(\boldsymbol{V}^+ - \boldsymbol{V}^-\right) = \tfrac{1}{2}\left(\boldsymbol{v}^+ - \boldsymbol{v}^-, \, z\left(\gamma^+ - \gamma^-\right) + \beta^+ - \beta^-\right) \tag{55}$$

and

$$\boldsymbol{J} = \nabla \times \boldsymbol{B}. \tag{56}$$

In (54) and(56) the curl is three dimensional.

We see that intense regions of $|\boldsymbol{U}|^2$ surround those of $|\boldsymbol{\Omega}|^2$. The former have dipole structures and the latter have monopole structures. The structure of $|\boldsymbol{\Omega}|^2$ makes a marked contrast with what we have for the Euler case, where petals of strong vorticity are interleaved

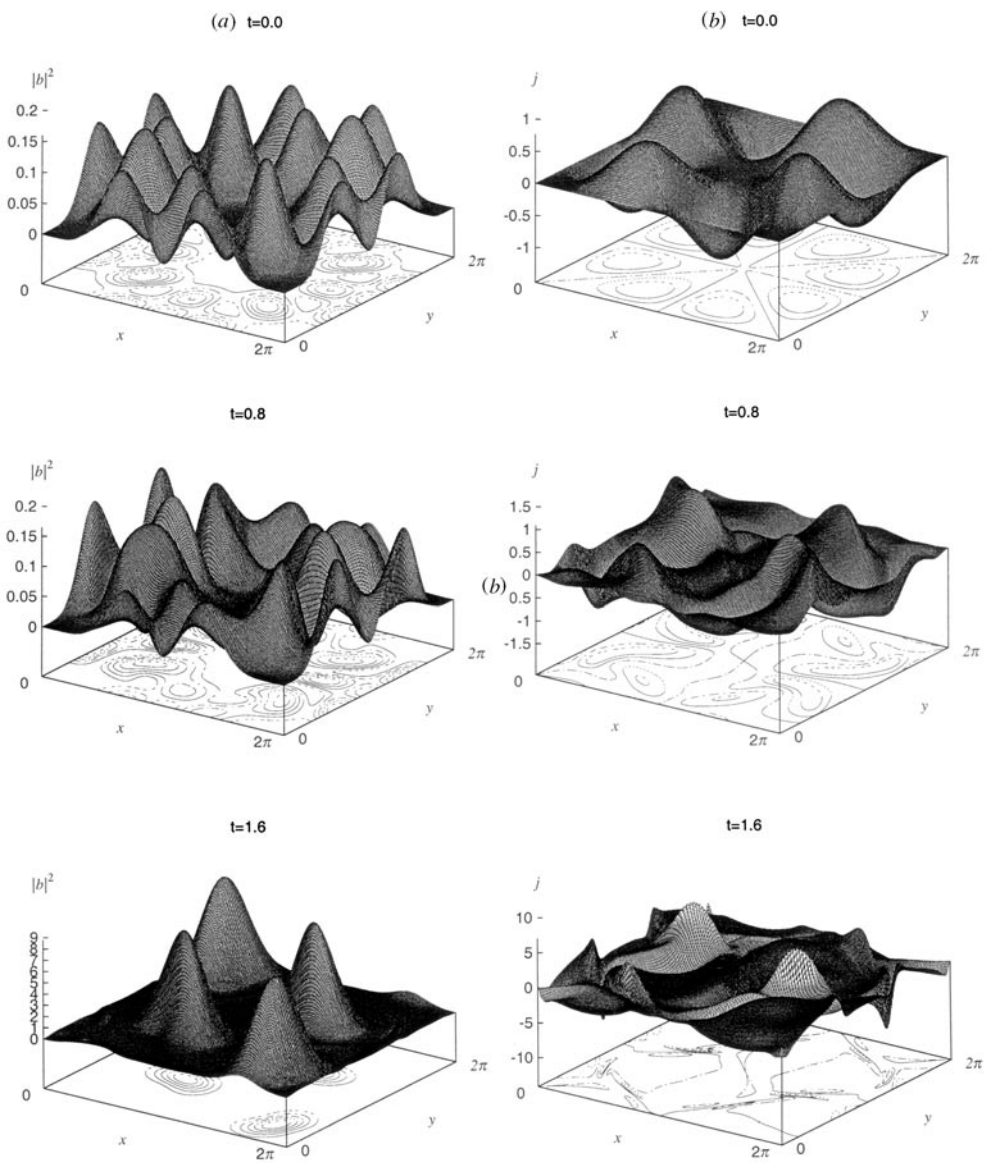

Figure 7. (*a*) The perspective plots of $|\boldsymbol{b}|^2$ at $t = 0, 0.8, 1.6$. (*b*) The perspective plots of j at $t = 0, 0.8, 1.6$.

with hollow regions of weak vorticity. In the present case of MHD, it has a maximum value at the centre of the core.

The monopole structure in $|\boldsymbol{B}|^2$ is induced by the dipole structure in $|\boldsymbol{J}|^2$. It should be noted that $\boldsymbol{B}$ is perpendicular to the z-axis. Therefore, in the regions where singularities are formed, $\boldsymbol{B}$ is orthogonal to $\boldsymbol{\Omega}$. We do not know, however, whether such a structure appears in finite energy MHD flows.

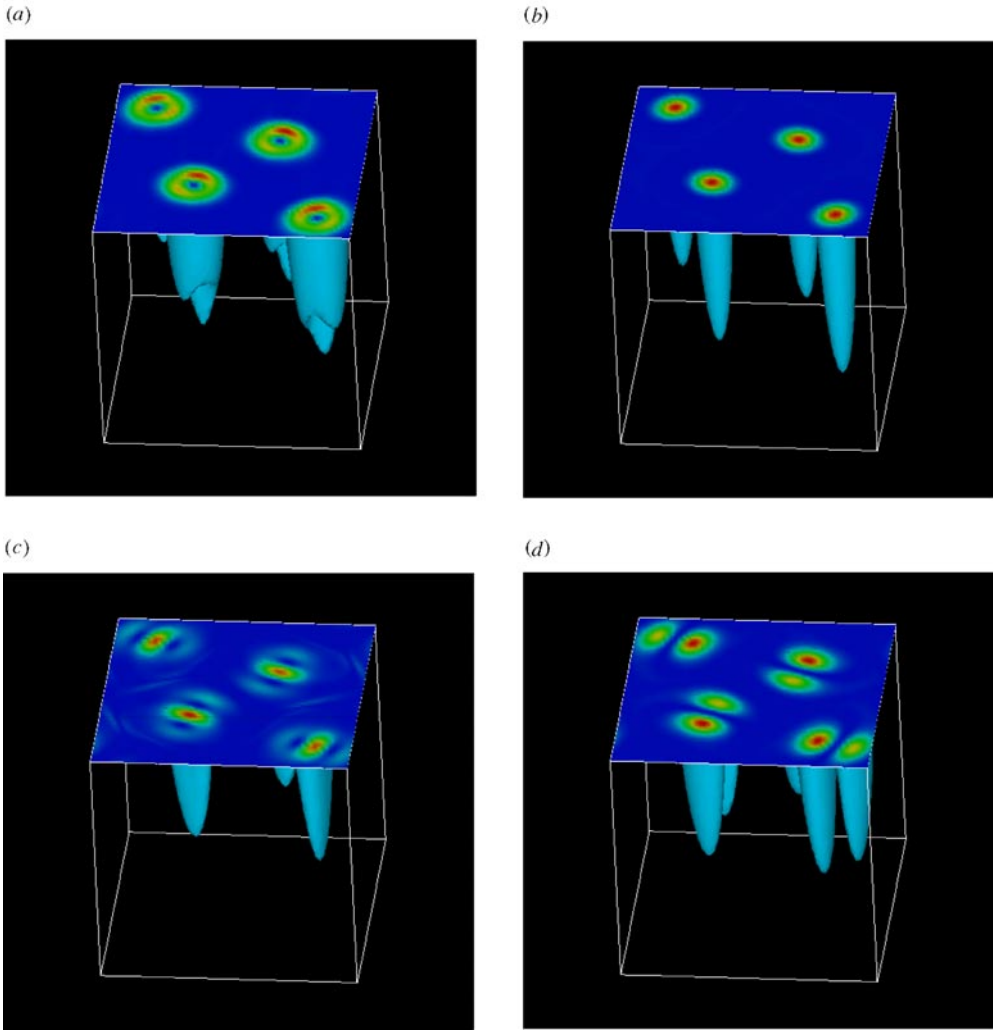

Figure 8. (*a*) The iso-surface of $|\boldsymbol{U}|^2$ in a box of $[0, 2\pi]^3$ with a cross sectional distribution on a plane $z = 2\pi$ at $t = 1.6$. Darker shading represents higher values. The threshold is set at one-fifth of the maximum value of $|\boldsymbol{U}|^2$. (*b*) Similar iso-surface of $|\boldsymbol{\Omega}|^2$ at $t = 1.6$. (*c*) Similar iso-surface of $|\boldsymbol{B}|^2$ at $t = 1.6$. (*d*) Similar iso-surface of $|\boldsymbol{J}|^2$ at $t = 1.6$.

To check that the resolution of numerical computations, the tail of the energy spectra of $\gamma^{\pm}$ was fitted in the form

$$E(k) \propto \exp(-2\delta k). \tag{57}$$

Even at $t = 1.6$ the fitted value of the analyticity distance was $\delta = 0.07 > 2\pi/N = 0.025$ ($N = 256$) (the fitting interval was $k \geqslant 10$), which indicates that the field is well resolved at that time.

We have also performed computations at higher resolutions. With $N = 512$ the numerical solution breaks down at $t = 1.613$ and with $N = 1024$ at $t = 1.599$; both of these are slightly earlier than the time of breakdown $t = 1.615$ at $N = 256$. A similar phenomenon has

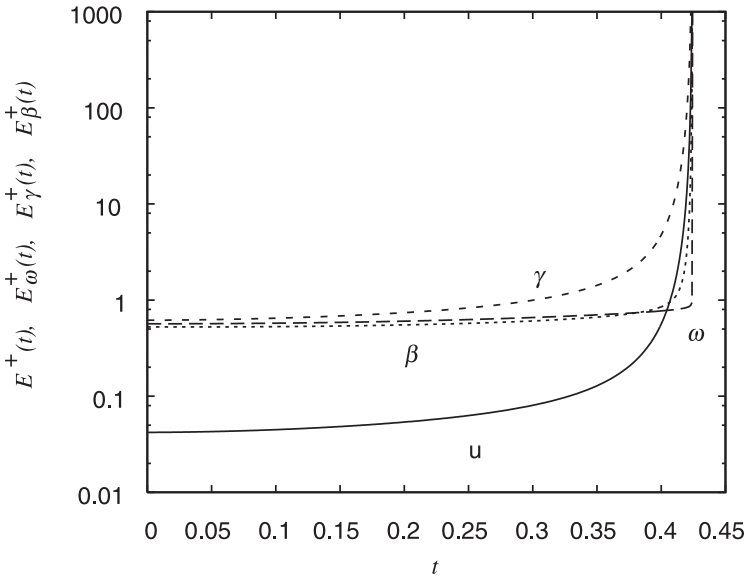

Figure 9. The time evolution of $E(t)$ (full), $E_\omega(t)$ (broken), $E_\gamma(t)$ (dashed) and $E_\beta(t)$ (dotted) for IC2.

been observed for the case of Euler equations [15] where the blow-up has been established theoretically [16].

We have attempted to use an adaptive step size control for time marching. However, this did not allow us to integrate further in time beyond the critical time encountered in computations with a fixed time step. We have also conducted the dissipative version of the calculation for this initial condition, where both viscosity and magnetic diffusivity take small but non-zero values $\nu = 1.0 \times 10^{-2}$. According to a preliminary computation, while the time of blow-up is delayed, e.g. $t = 1.7$ with $N = 512$, the singularity formation appears to persist in the viscous case. A similar phenomenon was reported briefly for the case of an ordinary fluid [15]. One possible interpretation is that unbounded velocity in the z-axis makes the nonlinear terms sufficiently strong to dominate the effect of the viscous term. However, details have yet to be investigated.

3.2. Random initial condition (IC 2)

It would be useful to see whether the qualitative understanding into the mechanism of singularity formation gained above using simple initial data helps when using a wider class. A more general initial datum is generated for each of $v_1^+,\ v_2^+,\ v_1^-,\ v_2^-$ by specifying their Fourier spectrum in the form

$$E(k) = C_1 k^4 \exp(-C_2 k^2). \tag{58}$$

The parameters are chosen as $C_1 = 1 \times 10^{-4}$ and $C_2 = 0.1$. The spectra for $\beta^+,\ \beta^-$ took the form $k^2 E(k)$, to make each term on the right-hand side of (22) comparable in magnitude. The phases of the Fourier coefficients have been randomized using different series of pseudo-random numbers so that no initial correlation exists between the fields.

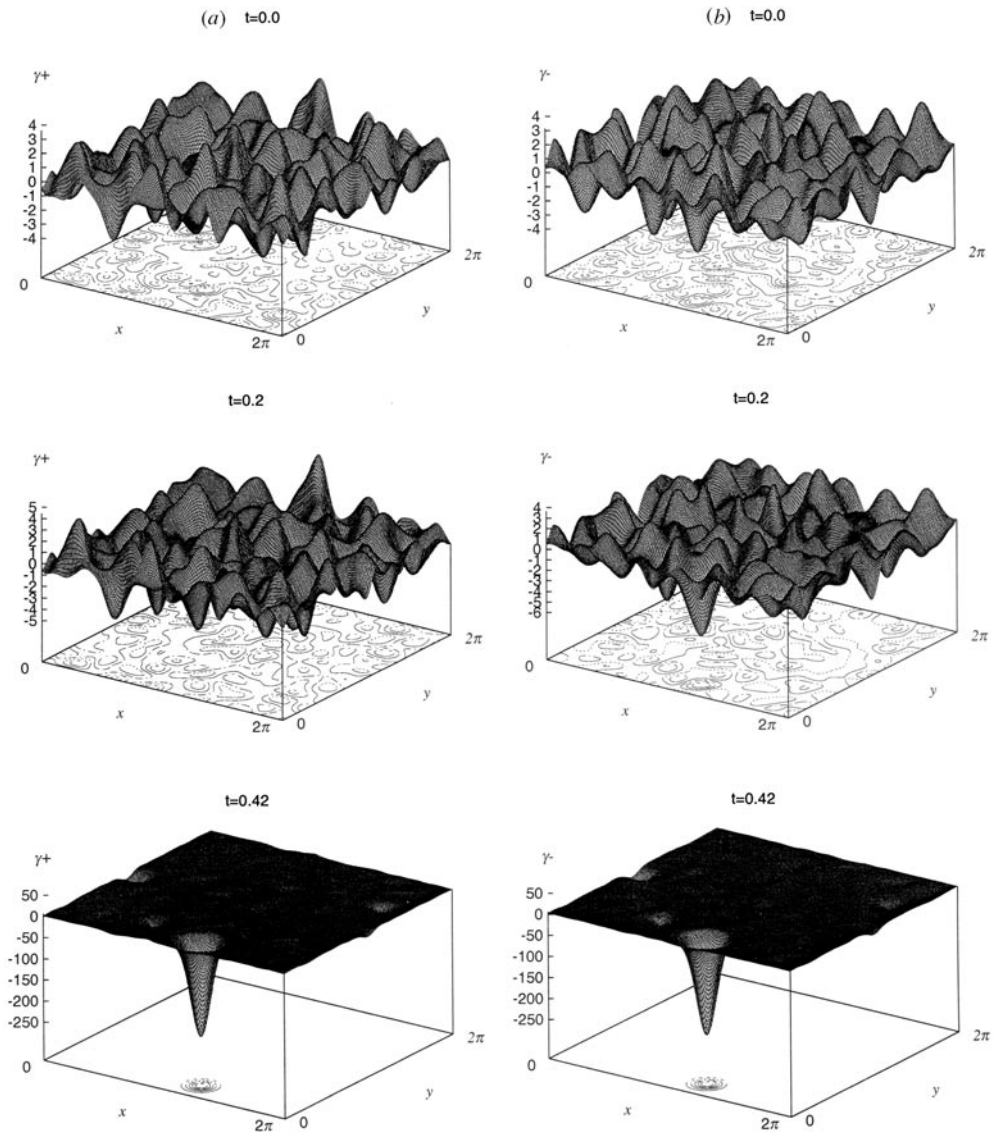

Figure 10. (*a*) The perspective plots of γ^+ at $t = 0, 0.2, 0.42$ for IC2. (*b*) Similar perspective plots of γ^-.

The time evolution of the norms for the + fields is shown in figure 9. All of them appear to blow up at $t = 0.42$. As in the case of IC1, $E(t)$ and $E_\gamma(t)$ start to grow at an early stage but $E_\omega(t)$ and $E_\beta(t)$ increase at a very late stage.

The time evolution of the perspective plots of γ^+ and γ^- are also shown in figures 10(*a*) and (*b*), respectively. Because the phase of the Fourier coefficients of $\gamma^\pm$ are randomized, no coherent structure exists initially and the two fields are uncorrelated. As time evolves, a prominent negative spike forms in γ^- at $t = 0.2$ and in γ^+ at a later stage $t = 0.3$ (not shown). It is remarkable that these spikes are located at the same position in the two-dimensional

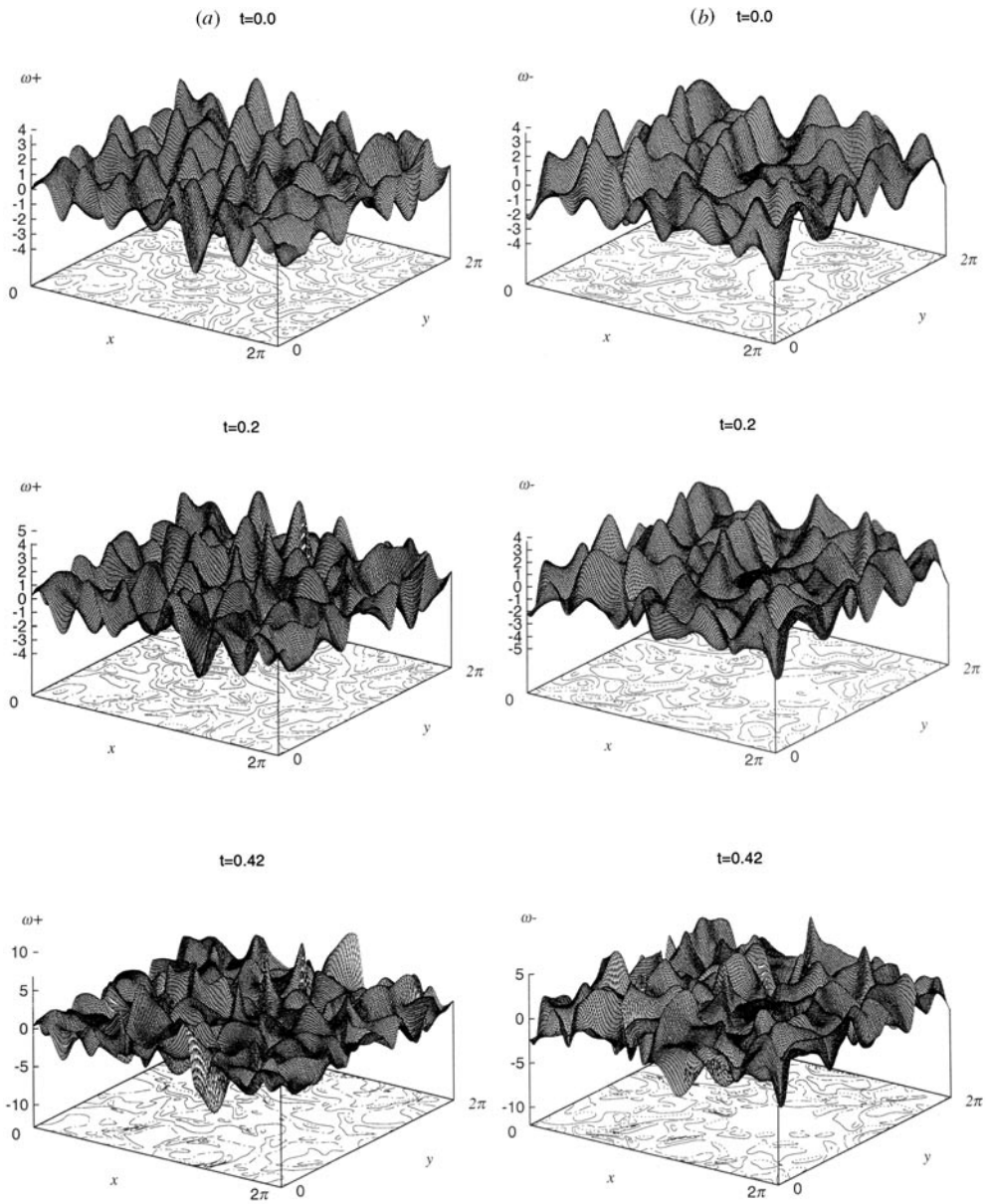

Figure 11. (*a*) The perspective plots of ω^+ at $t = 0, 0.2, 0.42$ for IC2. (*b*) Similar perspective plots of ω^-.

domain. At $t = 0.42$ the two fields γ^+ and γ^- look very similar. As in IC1, the correlation $C_\gamma(t)$ is close to unity at late times (figures omitted).

The time evolution of the perspective plots of ω^+ and ω^- are shown in figures 11(*a*) and (*b*), respectively. The field ω^+ apparently remains random up to $t = 0.4$ without any characteristic structure. Slightly later, however, at $t = 0.42$, platform-like structures of ω^+ appear, surrounding a region of strong spikes of $\gamma^\pm$. The same observation is also true for ω^-.

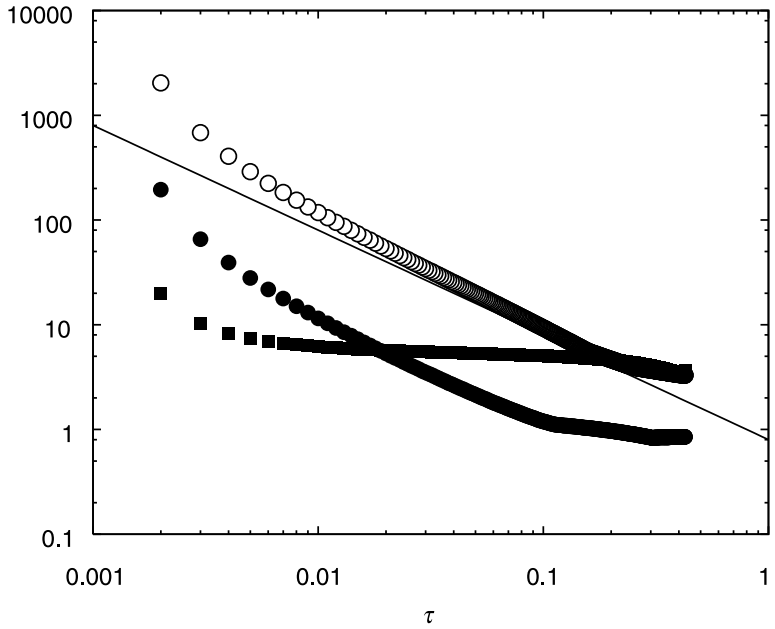

Figure 12. Time evolution of the maximum and minimum values: $\max_x |\boldsymbol{v}^+|(\boldsymbol{x}, t)$ (full squares), $\max_x \gamma^+(\boldsymbol{x}, t)$ (full circles), and $-\min_x \gamma^+(\boldsymbol{x}, t)$ (open squares). The full line represents a slope τ^{-1}.

This late formation of platform-like structures in vorticity is consistent with the slow growth of $E_\omega(t)$.

In figure 12 the time evolution of the maximum value of $|\boldsymbol{v}^+|$, and the maximum and minimum values of γ^+ are plotted against $\tau = t_* - t$ in a log–log plot. Again it is observed that the growth rate of γ^+ is stronger than $(t_* - t)^{-1}$, in agreement with the BKM-type criterion. That a similar property also holds for γ^- has also been confirmed. The maximum values of $\omega^\pm$ and $\beta^\pm$ have also been studied and these have been found to be similar to the results for IC1 (figures omitted).

In figure 13, $E_{\boldsymbol{u}}(t)$ and $E_{\boldsymbol{b}}(t)$ are shown. While they appear to blow up at the same time in the end, it is remarkable that $E_{\boldsymbol{b}}(t)$ remains almost constant except for the final stage, as in IC1. It has also been checked that growth of $\max_x |\boldsymbol{b}|$ is slower than that of $\max_x |\boldsymbol{u}|$ (figure omitted).

The normalized correlation coefficient between $\boldsymbol{u}$ and $\boldsymbol{b}$

$$C_{ub} = \frac{\int_{\mathcal{A}} \boldsymbol{u} \cdot \boldsymbol{b} \, \mathrm{d}\boldsymbol{x}}{\left(\int_{\mathcal{A}} |\boldsymbol{u}|^2 \, \mathrm{d}\boldsymbol{x} \int_{\mathcal{A}} |\boldsymbol{b}|^2 \, \mathrm{d}\boldsymbol{x} \right)^{1/2}} \tag{59}$$

is at most of the order of 0.03 and remains small all the time (figures omitted).

The numerical accuracy has been checked by estimating an analyticity strip. At $t = 0.4$ δ takes the value $\delta = 0.092$, whereas at a much later stage, $t = 0.42$, its value becomes $\delta = 0.087$. These are larger than the mesh size $\Delta = 2\pi/N = 0.025$.

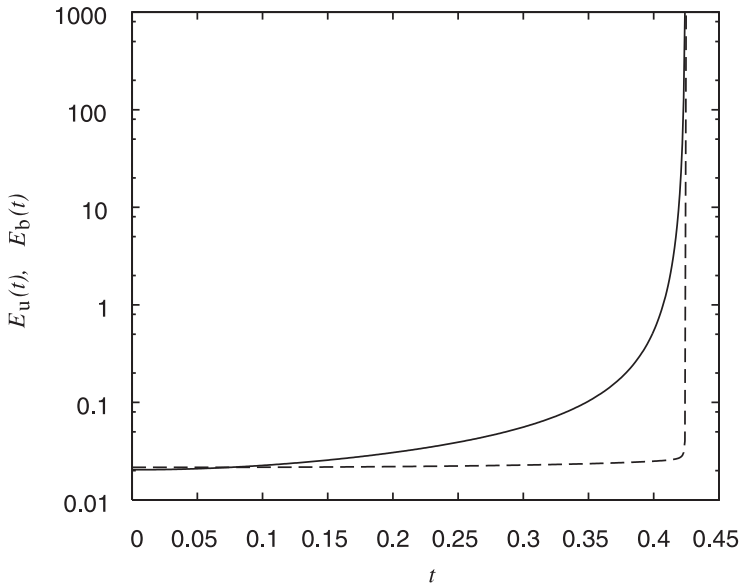

Figure 13. Time evolution of the total kinetic energy $E_u(t)$ (full) and magnetic energy $E_b(t)$ (broken) for IC2.

4. BKM-criteria that control singularities

4.1. A lemma on $\|\gamma^{\pm}\|_{\infty}$

Before proving a full BKM-type result, a subsidiary lemma can be proved that involves $\gamma^{\pm}$ alone.

Lemma 1. *At any time* $t^* > 0$*, the time integrals*

$$\int_0^{t^*} \|\gamma^+(\tau)\|_{\infty}\,\mathrm{d}\tau \qquad \textit{and} \qquad \int_0^{t^*} \|\gamma^-(\tau)\|_{\infty}\,\mathrm{d}\tau \tag{60}$$

must either both be bounded, in which case both $\|\gamma^+\|_{\infty}$ *and* $\|\gamma^-\|_{\infty}$ *are bounded at* t^**, or, if a singularity occurs at* t^**, then both integrals must become singular simultaneously.*

Remark. This result furnishes us with an analytical criterion that enables a numerical check to be made; for instance, the numerical results displayed in figure 5(*a*) of section 3 are consistent with the above lemma.

Proof. Let us consider the evolution of the L^{2m}-norms of $\gamma^{\pm}$. Define

$$I_{2m}^{\pm} = \int_{\mathcal{A}} |\gamma^{\pm}|^{2m}\,\mathrm{d}\boldsymbol{x} = \|\gamma^+\|_{2m}^{2m} \tag{61}$$

where L^2 is the area of $\mathcal{A}$. Then

$$\dot{I}_{2m}^{+} = 2m \int_{\mathcal{A}} (\gamma^+)^{2m-1} \left[-\boldsymbol{v}^- \cdot \nabla\gamma^+ - \gamma^+\gamma^- + 2L^{-2} \int_{\mathcal{A}} \gamma^+\gamma^-\,\mathrm{d}\boldsymbol{x} \right] \mathrm{d}\boldsymbol{x}. \tag{62}$$

Integrating the $\boldsymbol{v}^- \cdot \nabla \gamma^+$ term in the usual way we find that

$$\dot{I}^+_{2m} = -(2m+1)\int_{\mathcal{A}} \gamma^-(\gamma^+)^{2m}\,\mathrm{d}\boldsymbol{x} + 4mL^{-2}\left(\int_{\mathcal{A}} \gamma^+\gamma^-\,\mathrm{d}\boldsymbol{x}\right)\left(\int_{\mathcal{A}} (\gamma^+)^{2m-1}\,\mathrm{d}\boldsymbol{x}\right). \tag{63}$$

Hence, an application of Holder's inequality to the pair of integrals in the second term shows that the area cancels leaving

$$\dot{I}^+_{2m} \leqslant (6m+1)\|\gamma^-\|_\infty I^+_{2m}. \tag{64}$$

From (61) the time evolution of $\|\gamma^+\|_{2m}$ is

$$\frac{\mathrm{d}}{\mathrm{d}t}\|\gamma^+\|_{2m} \leqslant \left(\frac{6m+1}{2m}\right)\|\gamma^-\|_\infty \|\gamma^+\|_{2m} \tag{65}$$

and so in the limit $m \to \infty$,

$$\frac{\mathrm{d}}{\mathrm{d}t}\|\gamma^+\|_\infty \leqslant 3\,\|\gamma^-\|_\infty \|\gamma^+\|_\infty. \tag{66}$$

An integration with respect to time gives

$$\|\gamma^+(t)\|_\infty \leqslant \|\gamma^+(0)\|_\infty\, \exp\left(3\int_0^t \|\gamma^-(\tau)\|_\infty\,\mathrm{d}\tau\right) \tag{67}$$

with a more general result

$$\|\gamma^\pm(t)\|_\infty \leqslant \|\gamma^\pm(0)\|_\infty\, \exp\left(3\int_0^t \|\gamma^\mp(\tau)\|_\infty\,\mathrm{d}\tau\right). \tag{68}$$

Now consider the case, for instance, where $\int_0^t \|\gamma^-\|_\infty(\tau)\,\mathrm{d}\tau$ is finite. Then $\|\gamma^+\|_\infty$ must be finite by (68) even though $\|\gamma^-\|_\infty$ could (potentially) itself be singular. However, having established that $\|\gamma^+\|_\infty$ is finite, then its time integral must be finite also and so (68), with the opposite sign, shows that $\|\gamma^-\|_\infty$ must be finite too. Hence, any one of the two time integrals being finite means that the other one must also be finite and that both $\|\gamma^\pm\|_\infty$ are also finite. By the same argument, if one integral blows up then so must the other, because it is not possible to have one integral finite with the other singular. □

4.2. The main BKM result

The result of lemma 1 above is useful but says nothing about the possibility of singularities occurring in arbitrarily large gradients of $\gamma^\pm$ and $\boldsymbol{v}^\pm$. It is now possible to prove a result of the same type as that of Beale *et al* for the standard incompressible 3D Euler equations on an isotropic domain [1] and its extension to ideal MHD found by Caflisch *et al* [4]. Because equations (18)–(22) are expressed in two-dimensional variables only, it is necessary to find a criterion in terms of these without reference to z. Some modifications to the BKM proof are necessary but the principles remain the same. Hence we include only those elements that are different from standard Euler and Navier–Stokes analyses [1, 20–22].

Firstly, define the following two combinations of L^∞-norms:

$$\Gamma(t) = \|\gamma^+\|_\infty + \|\gamma^-\|_\infty + \|\omega^+\|_\infty + \|\omega^-\|_\infty \tag{69}$$

and

$$\Theta(t) = \|\gamma^+\|_\infty + \|\gamma^-\|_\infty + \|\nabla\boldsymbol{v}^+\|_\infty + \|\nabla\boldsymbol{v}^-\|_\infty \tag{70}$$

followed by the definitions

$$H_n^{\pm} = \int_{\mathcal{A}} |\nabla^n \boldsymbol{v}^{\pm}|^2 \, \mathrm{d}\boldsymbol{x} \tag{71}$$

and

$$H_n = H_n^+ + H_n^- \tag{72}$$

where ∇^n is the notation for the conventional multi-index derivative operation[3]. Two quantities involving gradients of $\gamma^{\pm}$ are also defined

$$G_n^{\pm} = \int_{\mathcal{A}} |\nabla^{n-1} \gamma^{\pm}|^2 \, \mathrm{d}\boldsymbol{x} \tag{73}$$

with

$$G_n = G_n^+ + G_n^-. \tag{74}$$

H_n and G_n have the same dimensions so it is appropriate to consider the sum of the two

$$F_n = H_n + G_n. \tag{75}$$

In fact, $H_1^{\pm}$ and $G_1^{\pm}$ are related by

$$H_1^{\pm} = \int_{\mathcal{A}} |\nabla \boldsymbol{v}^{\pm}|^2 \, \mathrm{d}\boldsymbol{x} = \int_{\mathcal{A}} \left(|\omega^{\pm}|^2 + |\gamma^{\pm}|^2 \right) \mathrm{d}\boldsymbol{x}. \tag{76}$$

The following theorem gives the criterion for control of F_n:

Theorem 1. *For $n \geqslant 1$, no F_n can become singular at a finite time $t^* > 0$ without $\int_0^{t^*} \Gamma(\tau) \, \mathrm{d}\tau$ also becoming singular. Contrapositively, if any F_n becomes singular at t^* then $\int_0^{t^*} \Gamma(\tau) \, \mathrm{d}\tau$ must also become singular.*

Proof. *Step 1.* Let us begin with the evolution of H_n^+

$$\begin{aligned} \tfrac{1}{2} \dot{H}_n^+ &= \int_{\mathcal{A}} \nabla^n \boldsymbol{v}^+ \cdot \nabla^n \left(\boldsymbol{v}^- \cdot \nabla \boldsymbol{v}^+ + \nabla P \right) \mathrm{d}\boldsymbol{x} \\ &\leqslant \tfrac{1}{2} \int_{\mathcal{A}} \gamma^- \left| \nabla^n \boldsymbol{v}^+ \right|^2 \mathrm{d}\boldsymbol{x} + c_n \left(\|\nabla \boldsymbol{v}^+\|_\infty + \|\nabla \boldsymbol{v}^-\|_\infty \right) H_n + \int_{\mathcal{A}} \nabla^n \boldsymbol{v}^+ \cdot \nabla^{n+1} P \, \mathrm{d}\boldsymbol{x}. \end{aligned} \tag{77}$$

The first and third terms on the right-hand side of (77) are normally zero in standard Navier–Stokes analysis when the velocity fields are divergence-free but here they need to be estimated

$$\tfrac{1}{2} \dot{H}_n \leqslant c_n \Theta(t) H_n + H_n^{1/2} \|\nabla^{n+1} P\|_2. \tag{78}$$

Noting that in L^2 an inequality of Calderon–Zygmund type [23] can be used

$$\|\nabla^{n+1} P\|_2 \leqslant c_n \|\nabla^{n-1} \Delta P\|_2 \tag{79}$$

equation (23) gives

$$\begin{aligned} \|\nabla^{n+1} P\|_2 &\leqslant c \left(\|\nabla^{n-1} \left(\gamma^+ \gamma^- \right)\|_2 + \sum_{i,j} \|\nabla^{n-1} \left(v_{i,j}^+ v_{j,i}^- \right)\|_2 \right) \\ &\leqslant c_n \Theta(t) \, F_n^{1/2} \end{aligned} \tag{80}$$

[3] Textbooks often use D^n but here ∇^n is used to avoid confusion with the material derivative $\mathrm{D}/\mathrm{D}t$.

Standard Gagliardo–Nirenberg inequalities [24] have been used to obtain (80). Altogether, (78) can be written as

$$\tfrac{1}{2}\dot{H}_n \leqslant c_n\,\Theta(t)\,F_n. \tag{81}$$

Using identical methods on G_n defined in (73) and (74), its time evolution is estimated by

$$\tfrac{1}{2}\dot{G}_n \leqslant c_n\,\Theta(t)\,F_n \tag{82}$$

Putting together the results of (81) and (82) for the evolution of H_n and G_n we find that

$$\tfrac{1}{2}\dot{F}_n \leqslant c_n\,\Theta(t)\,F_n. \tag{83}$$

Step 2. Clearly, equation (83) shows that $\int_0^t \Theta(\tau)\,\mathrm{d}\tau$ controls the growth of F_n. However, the point of the BKM theorem for 3D Euler is that it is the time integral of the L^∞-norm of the vorticity and not that of the velocity gradient matrix that is the key quantity that controls singularities [1]. Our desire here is for $\int_0^t \Theta(\tau)\,\mathrm{d}\tau$ to be replaced by $\int_0^t \Gamma(\tau)\,\mathrm{d}\tau$, as the theorem asserts. To achieve this it is necessary to appeal to a modified version of a logarithmic inequality first proved by Kato for the 2D Euler equations [19]. To estimate $\|\nabla \boldsymbol{v}^{\pm}\|_\infty$, account must be taken of the fact that the velocity fields $\boldsymbol{v}^{\pm}$ are not divergence-free and that boundary conditions are periodic. The latter just requires the use of standard extension theorems, as in [25]. Changes necessary to Kato's original proof [19] are minimal so these are omitted.

Lemma 2 (Kato [19]). *For $n \geqslant 3$*

$$\|\nabla \boldsymbol{v}^{+}\|_\infty + \|\nabla \boldsymbol{v}^{-}\|_\infty \leqslant c\,\Gamma(t)\;[1 + \ln(1 + F_3)]. \tag{84}$$

It is now clear that $\Theta(t)$ is controlled by $\Gamma(t)$ with a logarithmic correction in higher derivatives

$$\Theta(t) \leqslant c\,\Gamma(t)\;[1 + \ln(1 + F_3)]. \tag{85}$$

For $n \geqslant 3$, equation (83) becomes

$$\tfrac{1}{2}\dot{F}_n \leqslant c_n\,\Gamma(t) F_n\;[1 + \ln(1 + F_3)]. \tag{86}$$

Using the substitution $z = \log(1 + F_n)$ then $z(t)$ satisfies

$$z(t) \leqslant z(0) + c\int_0^t \Gamma(t)\big(1 + z(\tau)\big)\,\mathrm{d}\tau. \tag{87}$$

Gronwall's inequality then shows that the F_n are controlled by $\int_0^t \Gamma(\tau)\,\mathrm{d}\tau$. Hence no singularity can occur in any of the F_n if $\int_0^t \Gamma(\tau)\,\mathrm{d}\tau$ is bounded or, if a singularity does occur in any one of them at some time t^*, however, large n might be, then $\int_0^{t^*} \Gamma(\tau)\,\mathrm{d}\tau = \infty$. □

A final remark is that it is possible, from (22), to show that arbitrarily large gradients of $\beta^{\pm}$ are also controlled by $\int_0^{t^*} \Gamma(\tau)\,\mathrm{d}\tau$.

5. Conclusion

One of the main conclusions of this paper is that solutions of the type expressed in (4) for the equations for ideal MHD on a tubular domain produce similar but richer behaviour when compared with the three-dimensional Euler equations [15]. It was explained in [15] how these solutions of this type representing three-dimensional Euler flow in a tube or jet can be compared with those representing flows in a boundary layer [26, 27], where the stretching is

in two directions and not one. None of these flows are finite in energy (nor in helicity, in the case of ideal MHD) so they fall into a different category from the more familiar class of 3D finite domain flows whose energy and helicity are also finite.

Physically, the solutions displayed here for ideal MHD correspond to magnetic vortices that develop in the axial direction of the tube and which subsequently 'blow-up'. The blow-up process should not be taken as pointing to the existence of a true, physical, three-dimensional, finite time, infinite energy singularity: more realistically it points to how solutions of the type expressed in (4) grow violently and then become invalid after a finite time. In this sense, the behaviour of the class of solutions considered in this paper is significantly different from that of finite-energy MHD flows (see, for example, [5, 28]). Studies on this kind of class of solutions may show how the straining motion affects dynamics of the vorticity and/or magnetic fields prior to the singularity formation. These vortices and their breakdown may have some application to astrophysical jets and magnetic reconnection processes in circumstances where the equations of ideal MHD are applicable [6]. More specifically, it may be of interest to study in detail the relationship between singularity formation and the magnetic reconnection process in this class of stretched solutions. Any hints obtained in this way would be worth checking against conventional finite-energy MHD flows.

There are two areas where there are deficiencies in our treatment in comparison with the 3D Euler equations [15]. The first deficiency is analytical. Because of the doubling of the number of variables, there are two material derivatives in the Elsasser equations. In effect, this means there are two characteristics in the problem. Constantin's proof of blow-up for the Euler case rested on the existence of a single characteristic time in order to use a Lagrangian analysis [16]. In addition to this technical difficulty, the L^2-norms $\int_{\mathcal{A}} |\gamma|^2 \, \mathrm{d}\boldsymbol{x}$ in the Euler equations, whose signs are definite, are replaced by $\int_{\mathcal{A}} \gamma^+ \gamma^- \, \mathrm{d}\boldsymbol{x}$, whose signs are indefinite. This lack of definiteness makes a blow-up proof more difficult. So far we have been unable to surmount these difficulties.

The second deficiency lies in the numerical work; it was found to be difficult to track the growth of the magnetic field beyond a certain point. In the case of the first initial condition, this growth was no more than a factor of the order of 10 in amplification. Without corroborative analytical evidence such a relatively small growth factor would not normally be enough to claim as evidence for singular behaviour. The analytical evidence from section 2.3 than $\boldsymbol{b}$ must blow-up when $\gamma^{\pm} \to -\infty$ (for which the evidence is strong) is comforting but numerical calculations would be helpful that can track stronger growth in $\boldsymbol{b}$ closer to t_*.

Acknowledgments

JDG would like to thank the Research Institute for Mathematical Sciences (RIMS), Kyoto University, for the award of a Visiting Professorship from July 1st–October 1st 2000, during which period this work was carried out, and for the kind hospitality he received there. Part of this work has been supported by Grant-in-Aid nos 11304005 and 11214204 from the Ministry of Education, Science and Culture of Japan. We also thank the anonymous reviewers for useful comments.

References

[1] Beale J T, Kato T and Majda A 1984 Remarks on the breakdown of smooth solutions for the 3-D Euler equations *Commun. Math. Phys.* **94** 61–6

[2] Constantin P, Fefferman Ch and Majda A 1996 Geometric constraints on potentially singular solutions for the 3D Euler equations *Commun. Partial Differ. Equ.* **21** 559–71

[3] Kerr R 1993 Evidence for a singularity of the 3-dimensional, incompressible Euler equations *Phys. Fluids A* **5** 1725–46
[4] Caflisch R, Klapper I and Steele G 1997 Remarks on singularities, dimension and energy dissipation for ideal magneto-hydrodynamics *Commun. Math. Phys.* **184** 443–55
[5] Biskamp D 1993 *Nonlinear Magnetohydrodynamics* (Cambridge: Cambridge University Press)
[6] Priest E and Forbes T 2000 *Magnetic Reconnection* (Cambridge: Cambridge University Press)
[7] Kerr R and Brandenburg A 1999 Evidence for a singularity in ideal magnetohydrodynamics: implications for fast reconnection *Phys. Rev. Lett.* **83** 1155–58
[8] Grauer R and Marliani C 1998 Geometry of singular structures in magnetohydrodynamic flows *Phys. Plasmas* **5** 2544–52
[9] Grauer R and Marliani 2000 Current-sheet formation in 3D ideal incompressible magnetohydrodynamics *Phys. Rev. Lett.* **84** 4850–3
[10] Klapper I 1998 Constraints on finite-time current sheet formation at null points in two-dimensional ideal incompressible magnetohydrodynamics *Phys. Plasmas* **5** 910–4
[11] Cordoba D and Marliani C 2000 *Commun. Pure Appl. Math.* **53** 512–24
[12] Craik A D D 1988 A class of exact solutions in viscous incompressible magnetohydrodynamics *Proc. R. Soc.* A **417** 235–44
[13] Moffatt H K 1969 The degree of knottedness of tangled vortex lines *J. Fluid Mech.* **35** 117–29
[14] Gibbon J D, Fokas A and Doering C R 1999 Dynamically stretched vortices as solutions of the 3D Navier–Stokes equations *Physica* D **132** 497–510
[15] Ohkitani K and Gibbon J D 2000 Numerical study of singularity formation in a class of Euler and Navier–Stokes flows *Phys. Fluids* **12** 3181–94
[16] Constantin P 2000 The Euler equations and nonlocal conservative Riccati equations *Int. Math. Res. Not. (IMRN)* **9** 455–65
[17] Malham S J A 2000 Collapse of a class of three-dimensional Euler vortices *Proc. R. Soc.* **456** 2823–33
[18] Sulem P L, Frisch U, Pouquet A and Meneguzzi M 1985 On the exponential flattening of current sheets near neutral X-points in two-dimensional ideal MHD flow *J. Plasma Phys.* **33** 191–98
[19] Kato T 1986 Remarks on the Euler and Navier–Stokes equations in R^2 *Proc. Symp. Pure Math.* **45** 1–7
[20] Temam R 1988 *Infinite Dimensional Dynamical Systems in Mechanics and Physics* (New York: Springer)
[21] Constantin P and Foias C 1988 *Navier–Stokes Equations* (Chicago, IL: University of Chicago Press)
[22] Doering C R and Gibbon J D 1995 *Applied Analysis of the Navier–Stokes Equations* (Cambridge: Cambridge University Press)
[23] Gilbarg D and Trudinger N S 1998 *Elliptic Partial Differential Equations of Second Order* (Berlin: Springer)
[24] Nirenberg L 1959 On elliptic partial differential equations *Ann. Scuola Norm. Sup.* **13** 115–62
[25] Adams R 1975 *Sobolev Spaces* (New York: Academic)
[26] Stuart J T 1987 Nonlinear Euler partial differential equations: singularities in their solution *Proc. Symp. in Honour of C C Lin* (ed D J Benney, Chi Yuan and F H Shu) (Singapore, World Scientific) pp 81–95
[27] Childress S, Ierley S, Spiegel E and Young W 1989 Blow-up of unsteady two-dimensional Euler and Navier–Stokes solutions having stagnation point form *J. Fluid Mech.* **203** 1–22
[28] Biskamp D and Müller W-C 2000 Scaling properties of three-dimensional isotropic magnetohydrodynamic turbulence *Phys. Plasmas* **7** 4889–900